PROCEEDINGS OF THE ROYAL SOCIETY A

Proc. R. Soc. A (2007) **463**, 817–836
doi:10.1098/rspa.2006.1791
Published online 2 January 2007

Theory of four-point alternating current potential drop measurements on conductive plates

By John R. Bowler and Nicola Bowler*

Center for Nondestructive Evaluation, Iowa State University, 1915 Scholl Road, Ames, IA 50011-3042, USA

Measurements of alternating current potential drop (ACPD) made at the surface of a conductive plate can be used to determine, non-destructively, the parameters of the plate such as its thickness, electrical conductivity and linear effective magnetic permeability. In order to invert the measured potential drop to yield values for these parameters, a theoretical model is needed. In this work, closed form analytical expressions are derived for the ACPD measured between the two voltage electrodes of a four-point probe. Alternating current is injected and extracted by two current electrodes. The problem is formulated in terms of a single, transverse magnetic, potential. The exact solution for the electromagnetic field is expressed in terms of a Green's function for a plate via the method of images. The ACPD is also expressed as a sum of contributions from multiple images. Two series representations are given: one converges more rapidly for plates which are somewhat thicker than the probe dimensions and the other for plates which are somewhat thinner. Theoretical expressions for the ACPD in special cases of thick (half space) and thin conductors are shown to agree with the results presented previously. In this paper, calculated ACPD values are compared with the experimental data taken on a titanium plate, in the regime in which the plate thickness is similar to the probe length and excellent agreement is obtained.

Keywords: four-point probe; alternating current potential drop; metal plate characterization; electrical conductivity; magnetic permeability

1. Introduction

Multi-frequency alternating current potential drop (ACPD) measurements can be used to determine the linear electromagnetic material properties of a conductor, namely the electrical conductivity and effective permeability (Bowler & Huang 2005*a*). ACPD has provided the non-destructive evaluation community with a reliable method for crack sizing (Dover *et al.* 1981; Michael *et al.* 1982; Hwang & Ballinger 1992) and a means of monitoring crack growth during fatigue. In a four-point measurement, two current electrodes and two voltage electrodes are used. Typically, though not necessarily, they are arranged in a straight line and contact with the specimen is made using spring-loaded pins (figure 1). The potential drop is measured between the voltage electrodes.

* Author for correspondence (nbowler@iastate.edu).

Received 18 August 2006
Accepted 16 November 2006

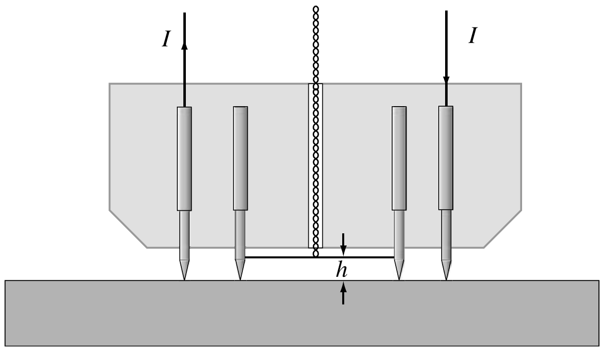

Figure 1. Four-point potential drop measurement system. Alternating current is applied to the specimen via the outer pair of spring-loaded pins. The potential drop is measured between the inner pair of pins.

The potential at a plate depends on the electrode location, plate thickness, frequency, conductivity and permeability. Absolute four-point measurement of conductivity can be achieved with the aid of a measurement theory which takes these factors into account. Within the limitations of an idealized model, in which the external current flows in thin wires normal to the surface of a homogeneous conductive plate and is injected or extracted at infinitesimal points on its surface, an exact expression for the field can be determined. The advantage of the exact theory is that one is not limited to making far field assumptions, thin-plate assumptions or a uniform local field approximation (Dover *et al.* 1981; Michael *et al.* 1982).

The four-point electromagnetic field in a half-space conductor has previously been derived from a solution expressed in terms of a transverse magnetic (TM) potential (Bowler 2004*a*). Predictions of the potential drop at the surface of the half space have been found from the field and compared with experimental measurements on thick plates (Bowler 2006*a*). The exact field for a homogeneous conductive plate of uniform thickness has also been found (Bowler 2004*b*) and comparisons between theory and experimental measurements of ACPD have been made using a thin-plate approximation (Bowler & Huang 2005*a*). Here, the TM potential formulation is used to express the exact field solution in terms of a Green's function for a plate. First, the Green's function for a half-space conductor is obtained and then that for the plate is derived using the method of images. The ACPD is similarly expressed as a sum of contributions from multiple images in the form of a series that converges rapidly for plates whose thickness is somewhat greater than the probe dimensions. The first term of this series is the half-space result presented in the work of Bowler (2006*a*). For plates somewhat thinner than the probe dimensions, an alternative series based on a Fourier representation is derived. It is shown how this solution reduces to the thin-plate solution presented in the work of Bowler & Huang (2005*a*).

In this paper, calculated ACPD voltage values are compared with the experimental data taken on a titanium plate whose thickness is approximately two-thirds of the probe length. For this measurement, neither the half-space solution nor the thin-plate solution describe the measurements satisfactorily. Rather, excellent agreement between the experimental data and the series solutions developed in this work is observed.

(a) Formulation

As described in the work of Bowler (2006a), the ACPD method measures a complex voltage, V, which has two contributions,

$$V = v + \varepsilon. \tag{1.1}$$

The first term, v, is the potential drop between the points on the plate at which the two voltage electrodes make contact with its surface. The source of v is the current in the plate injected by the two current electrodes. Generally, v is complex although, at sufficiently low frequency, v is predominantly resistive (real). The second term in equation (1.1), ε, is proportional to the inductance of the measurement circuit. It arises from the changing magnetic flux within the loop of the measurement circuit (whose height is h in figure 1) due to the time variation of the applied current, in this case of the form $\mathrm{e}^{-\mathrm{i}\omega t}$. ε is purely inductive (imaginary) and proportional to the frequency ω of the applied current and to the dimension h. ε tends to zero as the static limit of direct current is approached, where V is almost exclusively due to the conductor. The contribution from ε becomes larger, and eventually dominates, as ω increases. In order to infer the material parameters from a measurement of V, ε should be minimized by keeping h as small as possible. This can be achieved by connecting the pickup wires to the spring-loaded pins as close to the pin tips as possible and twisting the wires together in such a way as to minimize the area of the loop. Strictly, the quantities V, v, ε and $\boldsymbol{E}$ are complex amplitudes. For brevity, the time dependence is not shown explicitly in equation (1.1) or in the equations that follow.

(b) Direct current potential drop at a half-space conductor

First, consider a simple example, of direct current potential drop at a half-space conductor, which makes clear the structure of the solution for the more complicated cases that follow. In the case of direct current, $\varepsilon=0$ and the potential at a point on the surface of a half-space conductor due to direct current injected at one other point on the surface is inversely proportional to the distance between the injection and the measurement points, ρ. In fact,

$$V = \frac{I}{2\pi\sigma\rho}, \tag{1.2}$$

or

$$V = \frac{I}{2\pi\sigma} f(\rho), \tag{1.3}$$

with

$$f(\rho) = \frac{1}{\rho}. \tag{1.4}$$

In the case of a four-point probe, it is now easy to see that the potential drop between the pickup points may be written as the sum of four terms—the potential at each of the two measurement points due to the sources at the current injection and extraction points. With reference to figure 2,

$$V = V_1 - V_2 = \frac{I}{2\pi\sigma}[f(\rho_{22}) - f(\rho_{21}) - f(\rho_{12}) + f(\rho_{11})]. \tag{1.5}$$

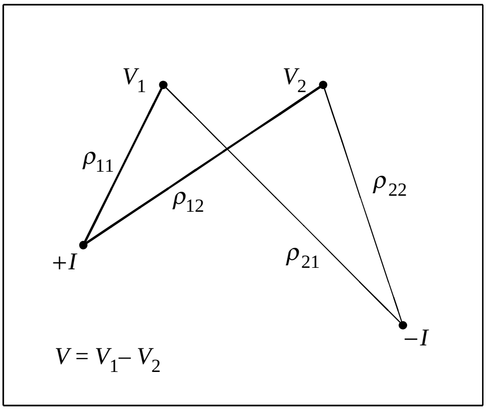

Figure 2. Arbitrary arrangement of the four electrode points on a conductor surface (plan view).

In this paper, exact and approximate forms of the function f are derived for alternating current injected into conductive half space and plate samples.

2. Calculation of ε

With reference to the discussion following equation (1.1), an expression for ε can be obtained by integrating the electric field around the loop of the measurement circuit whose height is h (figure 1), i.e.

$$\varepsilon = \oint \boldsymbol{E} \cdot \mathrm{d}\boldsymbol{l}. \tag{2.1}$$

For current injected into a conductor by a *single* wire held perpendicular to the conductor surface, the electric field in air on the same side of the plate as the wire may be expressed as the sum of contributions from the conductor itself, $\boldsymbol{E}^{\mathrm{c}}$, and the wire, $\boldsymbol{E}^{\mathrm{w}}$,

$$\boldsymbol{E}^{\mathrm{s}} = \boldsymbol{E}^{\mathrm{w}} + \boldsymbol{E}^{\mathrm{c}}, \quad \rho > 0,\ z \leq 0. \tag{2.2}$$

The electric field due to the wire can be easily obtained by application of Ampère's law, with the result

$$\boldsymbol{E}^{\mathrm{w}} = \hat{z}\frac{I}{2\pi}\mathrm{i}\omega\mu_0 \ln \rho, \quad \rho > 0,\ z \leq 0. \tag{2.3}$$

The contribution due to the conductor can be expressed in the following form, as derived in the work of Bowler (2004*b*):

$$\boldsymbol{E}^{\mathrm{c}} = \frac{I}{2\pi\sigma}\int_0^\infty \gamma \coth(\gamma c/2)\mathrm{e}^{\kappa z}[\hat{\rho}J_1(\kappa\rho) - \hat{z}J_0(\kappa\rho)]\mathrm{d}\kappa, \quad z \leq 0. \tag{2.4}$$

In equations (2.2)–(2.4), ρ and z are the variables of a cylindrical coordinate system centred on the current wire and $r^2 = \rho^2 + z^2$. In equation (2.4), $\gamma = \sqrt{\kappa^2 - k^2}$, where the root with positive real part is taken, and $J_i(x)$ is the ith-order Bessel function of the first kind. $k^2 = \mathrm{i}\omega\mu\sigma$, where μ is the magnetic permeability and σ is the electrical conductivity of the material. Here, note that

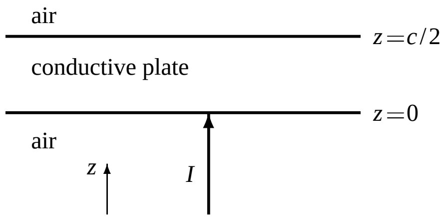

Figure 3. A current-carrying wire in contact with a conductive plate.

it can easily be shown that $\boldsymbol{E}^{\mathrm{c}}$ is conservative ($\nabla\times\boldsymbol{E}^{\mathrm{c}}=0$) and, therefore, does not contribute to the integral around the closed loop from which ε is derived (equation (2.1)). This means that only $\boldsymbol{E}^{\mathrm{w}}$ needs to be considered in the calculation of ε. In fact, this is true for both of the conductor geometries considered here (half space and plate), so ε has the same value for these cases.

For a system of *two* current-carrying wires in contact with the metal surface at coordinates $(x_1, y_1, 0)$ and $(x_2, y_2, 0)$, the electric field $\boldsymbol{E}$ can be obtained by superposition of the field due to a single wire,

$$\boldsymbol{E}(\boldsymbol{r}) = \boldsymbol{E}^{\mathrm{w}}(\boldsymbol{r}_1) - \boldsymbol{E}^{\mathrm{w}}(\boldsymbol{r}_2), \tag{2.5}$$

with $r_i=\sqrt{(x-x_i)^2+(y-y_i)^2+z^2}$, $i=1, 2$.

With equations (2.1) and (2.5),

$$\varepsilon = \oint[\boldsymbol{E}^{\mathrm{w}}(\boldsymbol{r}_1) - \boldsymbol{E}^{\mathrm{w}}(\boldsymbol{r}_2)]\cdot \mathrm{d}\boldsymbol{l}. \tag{2.6}$$

Considering the form of $\boldsymbol{E}^{\mathrm{w}}$, equation (2.3), evaluation of the integral in equation (2.6) is straightforward, yielding

$$\varepsilon = \frac{\mathrm{i}\omega\mu_0 hI}{2\pi}\ln\left(\frac{\rho_{22}\rho_{11}}{\rho_{21}\rho_{12}}\right), \tag{2.7}$$

or

$$\varepsilon = \frac{I}{2\pi\sigma}[f_\varepsilon(\rho_{22}) - f_\varepsilon(\rho_{21}) - f_\varepsilon(\rho_{12}) + f_\varepsilon(\rho_{11})], \tag{2.8}$$

where

$$f_\varepsilon(\rho) = \frac{h}{\mu_r}k^2\ln\rho, \tag{2.9}$$

and $\rho_{ij}=\sqrt{(x_i-x_j)^2+(y_i-y_j)^2}$ denotes the distance from source point i to voltage measurement point j.

3. Calculation of $\boldsymbol{v}$

(*a*) *Transverse magnetic potential formulation*

Consider the quasi-static electromagnetic field due to an alternating current injected into a half space ($z\geq 0$) or plate ($c/2\geq z\geq 0$) by a single conductive wire normal to the surface (figure 3). (In the mathematical development, the conductor is located in the space defined by $z>0$ for algebraic convenience.) In such an arrangement, the field is TM with respect to the direction of the normal to the surface ($\hat{z}$) and hence can be expressed as

$$\boldsymbol{H} = \nabla \times [\hat{z}\psi], \tag{3.1}$$

where $\boldsymbol{H}$ is the magnetic field and ψ is the TM potential. This expression represents the fact that the magnetic field has no z-component. (That this is true can be seen more easily by considering the electric field, $\boldsymbol{E}$. With respect to a cylindrical coordinate system whose axis coincides with the wire, $\boldsymbol{E}_r$ does not depend on the azimuthal angle and $\boldsymbol{E}_\phi = 0$. Hence, the z-component of the curl of the electric field, which is $\mathrm{i}\omega\mu H_z$, is zero.) From Ampère's law, the quasi-static electric current density is

$$\boldsymbol{J} = \nabla \times \nabla \times [\hat{z}\psi]. \tag{3.2}$$

Assuming that the field varies in time as the real part of $\exp(-\mathrm{i}\omega t)$, the magnetic field satisfies

$$\nabla \times \nabla \times \boldsymbol{H} - k^2 \boldsymbol{H} = 0, \tag{3.3}$$

where $k = \sqrt{\mathrm{i}\omega\mu\sigma}$, taking the root with a positive real part. In the non-conductive region, $k=0$. A governing equation for the TM potential can be obtained by substituting the magnetic field expression in equation (3.1) into equation (3.3), using the relation

$$\nabla \times \nabla \times \equiv \nabla\nabla\cdot - \nabla^2, \tag{3.4}$$

then operating with $\hat{z}\times$ followed by the transverse divergence ∇_t, where the differential operator transverse to the $\hat{z}$-direction is given by

$$\nabla_t = \nabla - \hat{z}\frac{\partial}{\partial z}. \tag{3.5}$$

This gives

$$(\nabla^2 + k^2)\nabla_t^2 \psi = 0. \tag{3.6}$$

Now define a new potential, Ψ, as follows:

$$\nabla_t^2 \psi(\rho, z) = \Psi(\rho, z), \tag{3.7}$$

which, from equation (3.6), obeys the Helmholtz equation

$$(\nabla^2 + k^2)\Psi = 0, \tag{3.8}$$

and seek a solution for Ψ that vanishes far from the injection point.

(b) Boundary conditions

To determine the boundary conditions, other than the far field requirement, note from equation (3.2) that

$$J_z = -\nabla_t^2 \psi = -\Psi. \tag{3.9}$$

Assuming that current is injected and extracted at a surface $z=0$, then $J_z(\rho, 0_+)=0$, and $\Psi(\rho, 0_+)=0$ at every point except the point or points where current is injected or extracted. In the idealization that considers the current injected at an infinitesimal point, it is appropriate to use a delta function to represent the normal surface current density. In order to determine the strength of the delta-function source, an axially symmetric injection current distributed over a finite disc with radius ρ_0 is first considered. The current flowing into the conductor through this surface region can be written in terms of an integral over the current density as follows:

$$I = 2\pi \int_0^{\rho_0} J_z(\rho, 0_+)\rho \,\mathrm{d}\rho, \tag{3.10}$$

where I is the total current. For extraction or injection at a point, we express the current density in terms of a delta function $\delta(\rho)$ with the property

$$\int_0^{\rho_0} \delta(\rho)\mathrm{d}\rho = 1,$$

for any positive ρ_0. Thus, for equation (3.10) to hold with the delta-function representation of the current density,

$$J_z(\rho, 0_+) = \frac{I}{2\pi}\delta(\rho)/\rho.$$

The boundary condition on the potential is therefore

$$\Psi(\rho, 0_+) = -\frac{I}{2\pi}\delta(\rho)/\rho. \tag{3.11}$$

From relation (3.7), boundary condition (3.11) implies that

$$\psi(\rho, 0_+) = -\frac{I}{2\pi}\ln \rho. \tag{3.12}$$

So, ψ does not vanish as $\rho \to \infty$ but, when a second contact point is added for current extraction creating a dipolar source, the far-field vanishing condition is satisfied. In a conductive half space ($z>0$), it is also required that the potential vanishes as $z \to \infty$. Later, when considering the case of a plate with no current injection or extraction points on the upper surface ($z=c/2$), it will also be required that Ψ and ψ vanish on the upper surface. First, however, the solution for a half-space conductor will be obtained to provide a foundation on which to build the plate solution.

(c) *Half-space Green's function solution for* Ψ

A solution of Helmholtz equation (3.8) is sought in the case of a half-space conductor using a Green's function that satisfies

$$(\nabla^2 + k^2)G(\boldsymbol{r}, \boldsymbol{r}') = -\delta(\boldsymbol{r} - \boldsymbol{r}'). \tag{3.13}$$

The unbounded domain solution of equation (3.13) which vanishes in the far field, also known as the fundamental solution, is

$$G_0(\boldsymbol{r}, \boldsymbol{r}') = \frac{\exp\left[\mathrm{i}k\sqrt{\rho^2 + (z - z')^2}\right]}{4\pi\sqrt{\rho^2 + (z - z')^2}}, \tag{3.14}$$

where $\rho^2 = (x - x')^2 + (y - y')^2$. For a half space, a Green's function which satisfies the same boundary condition as the TM potential is needed, except for the fact that the current injection or extraction point at the surface does not feature, i.e. $G(\boldsymbol{r},\boldsymbol{r}')=0$ at $z=0$. From the method of images, it is immediately clear that the following expression:

$$G(\boldsymbol{r},\boldsymbol{r}') = \frac{\exp\left[\mathrm{i}k\sqrt{\rho^2+(z-z')^2}\right]}{4\pi\sqrt{\rho^2+(z-z')^2}} - \frac{\exp\left[\mathrm{i}k\sqrt{\rho^2+(z+z')^2}\right]}{4\pi\sqrt{\rho^2+(z+z')^2}}, \tag{3.15}$$

satisfies equation (3.13) and vanishes at $z=0$. Now, Green's second theorem may be invoked to find a relationship between $\Psi(\boldsymbol{r})$ and $G(\boldsymbol{r},\boldsymbol{r}')$. Green's second theorem may be written as follows:

$$\int_\Omega G(\boldsymbol{r}',\boldsymbol{r})\nabla'^2\Psi(\boldsymbol{r}') - \Psi(\boldsymbol{r}')\nabla'^2 G(\boldsymbol{r}',\boldsymbol{r})\mathrm{d}\boldsymbol{r}'$$

$$= \int_S G(\boldsymbol{r}',\boldsymbol{r})\frac{\partial\Psi(\boldsymbol{r}')}{\partial n'} - \Psi(\boldsymbol{r}')\frac{\partial G(\boldsymbol{r}',\boldsymbol{r})}{\partial n'}\mathrm{d}S', \tag{3.16}$$

where the surface S here lies within the conductor, enclosing the half-space conductive region, Ω. The coordinate in the direction of the outward normal to this surface is n'. Applying equations (3.8) and (3.13) to the left-hand side of equation (3.16), the term in the integrand which contains the delta function survives to give $\Psi(\boldsymbol{r})$, whereas other terms cancel. On the right-hand side of equation (3.16), the first term vanishes since $G(\boldsymbol{r},\boldsymbol{r}')=0$ on S. Hence,

$$\Psi(\boldsymbol{r}) = \int_{S_0} \Psi(\boldsymbol{r}')\frac{\partial G(\boldsymbol{r}',\boldsymbol{r})}{\partial z'}\mathrm{d}S', \tag{3.17}$$

where S_0 represents the surface at $z=0$. Note that a negative sign has vanished because the positive z-direction is opposite to that of the outward normal from S_0. Further, using equation (3.11),

$$\Psi(\boldsymbol{r}) = -I\left[\frac{\partial G(\boldsymbol{r}',\boldsymbol{r})}{\partial z'}\right]_{z'=0} = 2I\left[\frac{\partial G_0(\boldsymbol{r},\boldsymbol{r}')}{\partial z}\right]_{z'=0}, \tag{3.18}$$

gives the solution sought,

$$\Psi = \frac{I}{2\pi}\frac{z}{(\rho^2+z^2)^{3/2}}\left(\mathrm{i}k\sqrt{\rho^2+z^2}-1\right)\mathrm{e}^{\mathrm{i}k\sqrt{\rho^2+z^2}}. \tag{3.19}$$

Allowing for the differences in notation, this result is in agreement with eqn (32) in the work of Bowler (2004*a*). Next, it is shown how the potential drop for a half-space conductor, v_{hs}, is determined from this result.

(*d*) *Half-space potential drop*, v_{hs}

Combining the following statement of Ohm's law, which relates the current density and the electric field,

$$\boldsymbol{J} = \sigma\boldsymbol{E}, \tag{3.20}$$

with relationship (3.2), and applying identities (3.4) and (3.5), it can be seen that

$$\boldsymbol{E}_t = \frac{1}{\sigma}\nabla_t\frac{\partial\psi}{\partial z}. \tag{3.21}$$

Hence, the potential v at a point Q_1 relative to that at another point Q_2, both in the plane $z=0$, is found by integrating equation (3.21) from Q_2 to Q_1,

$$v = \frac{1}{\sigma}\left[\frac{\partial \psi}{\partial z}\bigg|_{Q_1} - \frac{\partial \psi}{\partial z}\bigg|_{Q_2}\right]. \tag{3.22}$$

Evidently, the ACPD can be computed directly from $\partial\psi/\partial z$. The function ψ can be found from the solution for Ψ by integration of equation (3.7). Since

$$\nabla_t^2 \psi = \nabla_t \cdot \nabla_t \psi = \left(\frac{\hat{\rho}}{\rho}\frac{\partial}{\partial \rho}\rho\right)\cdot\left(\hat{\rho}\frac{\partial \psi}{\partial \rho}\right) = \Psi,$$

it follows that

$$\frac{\partial \psi}{\partial \rho} = \frac{1}{\rho}\int \rho \Psi \,\mathrm{d}\rho = \frac{I}{2\pi\rho}\int \frac{\partial}{\partial z}\frac{\mathrm{e}^{\mathrm{i}k\sqrt{\rho^2+z^2}}}{\sqrt{\rho^2+z^2}}\rho \,\mathrm{d}\rho$$

where equation (3.18), with equation (3.14), has been used. Putting $r=\sqrt{\rho^2+z^2}$ and $\rho \,\mathrm{d}\rho = r\,\mathrm{d}r$ gives

$$\frac{\partial \psi}{\partial \rho} = \frac{I}{2\pi\rho}\int z\left(\frac{\mathrm{i}k}{r} - \frac{1}{r^2}\right)\mathrm{e}^{\mathrm{i}kr}\mathrm{d}r.$$

Using the following definition of the exponential integral function E_1 (Gradshteyn & Ryzhik 2000), eqn (2.325.1):

$$\int \frac{\mathrm{e}^{ar}}{r}\mathrm{d}r = -E_1(-ar),$$

and the identity (Gradshteyn & Ryzhik 2000), eqn (2.325.2),

$$\int \frac{\mathrm{e}^{ar}}{r^2}\mathrm{d}r = -\frac{\mathrm{e}^{ar}}{r} - aE_1(-ar),$$

gives

$$\frac{\partial \psi}{\partial \rho} = \frac{I}{2\pi\rho}\left[\frac{z}{\sqrt{\rho^2+z^2}}\mathrm{e}^{\mathrm{i}k\sqrt{\rho^2+z^2}} - \mathrm{e}^{\mathrm{i}kz}\right], \tag{3.23}$$

in agreement with eqn (38) in the work of Bowler (2004*a*). The integration introduces an additive function independent of ρ chosen to be $\exp(\mathrm{i}kz)$ in order to eliminate a singularity at $\rho=0$. As a result, equation (3.23) contains two terms with singularities at $\rho=0$, which cancel except at $z=0$ where the result is consistent with equation (3.12).

Now integrate expression (3.23) with respect to ρ, to find

$$\psi = \frac{I}{2\pi}\left[\int \frac{z}{\rho\sqrt{\rho^2+z^2}}\mathrm{e}^{\mathrm{i}k\sqrt{\rho^2+z^2}}\mathrm{d}\rho - \mathrm{e}^{\mathrm{i}kz}\ln \rho\right].$$

Putting $r=\sqrt{\rho^2+z^2}$ in the integral, we have

$$\int \frac{z}{r^2-z^2}\mathrm{e}^{\mathrm{i}kr}\mathrm{d}r = \frac{1}{2}\int\left(\frac{1}{r-z} - \frac{1}{r+z}\right)\mathrm{e}^{\mathrm{i}kr}\mathrm{d}r$$
$$= -\frac{1}{2}\{\mathrm{e}^{\mathrm{i}kz}E_1[-\mathrm{i}k(r-z)] - \mathrm{e}^{\mathrm{i}kz}E_1[-\mathrm{i}k(r+z)]\}.$$

Hence,

$$\psi = -\frac{I}{2\pi}\left(\frac{1}{2}\{\mathrm{e}^{\mathrm{i}kz}E_1[-\mathrm{i}k(r-z)] - \mathrm{e}^{-\mathrm{i}kz}E_1[-\mathrm{i}k(r+z)]\} + \mathrm{e}^{\mathrm{i}kz}\ln \rho\right), \tag{3.24}$$

and, by differentiating with respect to z, the following is obtained:

$$\frac{\partial\psi}{\partial z} = -\frac{I}{2\pi}\left(\frac{e^{ikr}}{r} + ik\left\{\frac{e^{ikz}}{2}E_1[-ik(r-z)] + \frac{e^{-ikz}}{2}E_1[-ik(r+z)] + e^{ikz}\ln\rho\right\}\right). \tag{3.25}$$

Further, at the surface $z=0$,

$$\left.\frac{\partial\psi}{\partial z}\right|_{z=0} = -\frac{I}{2\pi}\left\{\frac{e^{ik\rho}}{\rho} + ik[E_1(-ik\rho) + \ln\rho]\right\}, \tag{3.26}$$

which is in agreement with the half-space ACPD given by eqn (19) in the work of Bowler (2006*a*). Thus, the potential drop can be written in the form of equation (1.5),

$$v_{hs} = \frac{I}{2\pi\sigma}[f_{hs}(\rho_{22}) - f_{hs}(\rho_{21}) - f_{hs}(\rho_{12}) + f_{hs}(\rho_{11})], \tag{3.27}$$

where

$$f_{hs}(\rho) = \frac{e^{ik\rho}}{\rho} + ik[E_1(-ik\rho) + \ln\rho]. \tag{3.28}$$

(*e*) *Plate solution*

For a plate of thickness $c/2$, an additional boundary condition is needed on the back surface of the plate,

$$\Psi(\rho, c/2) = 0 \quad \text{and} \quad \psi(\rho, c/2) = 0. \tag{3.29}$$

Then, according to elementary image theory, Green's function is

$$G(\boldsymbol{r}, \boldsymbol{r}') = \sum_n \frac{\exp\left[ik\sqrt{\rho^2 + (z - z' + nc)^2}\right]}{4\pi\sqrt{\rho^2 + (z - z' + nc)^2}} - \frac{\exp\left[ik\sqrt{\rho^2 + (z + z' - nc)^2}\right]}{4\pi\sqrt{\rho^2 + (z + z' - nc)^2}}, \tag{3.30}$$

where the summation here and elsewhere is from $-\infty$ to $+\infty$ unless otherwise stated. Proceeding as in the case of the half-space solution, the following counterpart to equation (3.18) is obtained:

$$\Psi(\boldsymbol{r}) = 2I\sum_n \left[\frac{\partial G_0(\boldsymbol{r}, \boldsymbol{r}' - nc)}{\partial z}\right]_{z'=0}. \tag{3.31}$$

In place of the half-space result, equation (3.19),

$$\Psi = \frac{I}{2\pi}\sum_n \frac{z + nc}{[\rho^2 + (z + nc)^2]^{3/2}}\left[ik\sqrt{\rho^2 + (z + nc)^2} - 1\right]e^{ik\sqrt{\rho^2 + (z+nc)^2}}. \tag{3.32}$$

Following the steps detailed in §3*d* and putting $z_n = z + nc$ and $r_n = \sqrt{\rho^2 + (z + nc)^2}$ to obtain a more compact expression, we obtain

$$\psi = -\frac{I}{2\pi}\sum_n\left(\frac{1}{2}\{e^{ikz_n}E_1[-ik(r_n - z_n)] - e^{-ikz_n}E_1[-ik(r_n + z_n)]\}\right.$$
$$\left. + \operatorname{sgn}(z - nc)e^{ik|z_n|}\ln\rho\right), \tag{3.33}$$

whose half-space counterpoint is given in equation (3.24). Equation (3.33) has been written in such a way that the domain of ψ has been extended to infinity, to include all of the virtual images. In this extended space, ψ is periodic (odd) in z with period c, which is the reason for the factor $\mathrm{sgn}(z-nc)$. The last term in equation (3.33) is introduced to eliminate singularities at $\rho=0$, as explained in the discussion following equation (3.23) in the case of the half space.

Further, ψ can also be expanded as a cosine series which converges rapidly when c is small. This line of development is taken up in §3*f* below.

Taking the derivative of ψ with respect to z gives

$$\frac{\partial \psi}{\partial z} = -\frac{I}{2\pi}\sum_n \left(\frac{\mathrm{e}^{\mathrm{i}kr_n}}{r_n} + \mathrm{i}k\left\{\frac{\mathrm{e}^{\mathrm{i}kz_n}}{2}E_1[-\mathrm{i}k(r_n - z_n)] + \frac{\mathrm{e}^{-\mathrm{i}kz_n}}{2}E_1[-\mathrm{i}k(r_n + z_n)] + \mathrm{e}^{\mathrm{i}k|z_n|}\ln\rho\right\}\right), \tag{3.34}$$

and, at the plane $z=0$,

$$\left.\frac{\partial \psi}{\partial z}\right|_{z=0} = \frac{I}{2\pi}\left[\mathrm{i}k\coth\left(\frac{\mathrm{i}kc}{2}\right)\ln\rho - \sum_n\left(\frac{\exp\left[\mathrm{i}k\sqrt{\rho^2+(nc)^2}\right]}{\sqrt{\rho^2+(nc)^2}} + \mathrm{i}k\,\mathrm{e}^{\mathrm{i}knc}E_1\left\{-\mathrm{i}k\left[\sqrt{\rho^2+(nc)^2}-nc\right]\right\}\right)\right], \tag{3.35}$$

where the geometric series has been summed with result

$$\sum_n \exp(\mathrm{i}k|nc|) = -\mathrm{i}k\coth(\mathrm{i}kc/2).$$

Thus, the potential drop can be written

$$v_\mathrm{p} = \frac{I}{2\pi\sigma}[f_\mathrm{p}(\rho_{22}) - f_\mathrm{p}(\rho_{21}) - f_\mathrm{p}(\rho_{12}) + f_\mathrm{p}(\rho_{11})], \tag{3.36}$$

where

$$f_\mathrm{p}(\rho) = -\mathrm{i}k\coth\left(\frac{\mathrm{i}kc}{2}\right)\ln\rho + \sum_n\left(\frac{\exp\left[\mathrm{i}k\sqrt{\rho^2+(nc)^2}\right]}{\sqrt{\rho^2+(nc)^2}} + \mathrm{i}k\,\mathrm{e}^{\mathrm{i}knc}E_1\left\{-\mathrm{i}k\left[\sqrt{\rho^2+(nc)^2}-nc\right]\right\}\right). \tag{3.37}$$

In the limit in which $c\to\infty$, $\coth(\mathrm{i}kc/2)\to -1$ and in the summations only the term with $n=0$ survives so that the half-space result given in equation (3.28) is recovered.

The series in equation (3.37) converges rapidly for thick plates. In the work of Bowler (2006*b*), the accuracy of asymptotic half-space expression (3.28) is investigated thoroughly in the limit of direct current. The results of the investigation are also applicable for frequencies below a certain threshold frequency, f_s (Bowler & Huang 2005*a*), which bounds a quasi-static regime in which the measured voltage is predominantly real and approximately constant. For thin plates, it is more computationally efficient to use an alternative series representation, described in §3*f*.

(*f*) *Fourier series representation for the plate solution*

It is possible to make use of the following identity (Sperb 1996):

$$\sum_n \frac{\exp\left[\mathrm{i}k\sqrt{\rho^2+(z+nc)^2}\right]}{\sqrt{\rho^2+(z+nc)^2}} = \frac{2}{c}K_0(-\mathrm{i}k\rho) + \frac{4}{c}\sum_{\nu=1}^{\infty} K_0\left[(\rho/c)\sqrt{(2\pi\nu)^2-(kc)^2}\right]\cos(2\pi\nu z/c), \tag{3.38}$$

to obtain an alternative expression for the result expressed in equations (3.36) and (3.37). In equation (3.38), $K_0(z)$ is the modified Bessel function of the second kind, of order zero. Casting the plate Green's function of equation (3.30) in the form of equation (3.38) and using relations (3.7) and (3.31) give

$$\begin{aligned}\frac{\partial\psi}{\partial z} &= 2I\nabla_t^{-2}\sum_n\left[\frac{\partial^2 G_0(\boldsymbol{r}|\boldsymbol{r}'-nc)}{\partial z^2}\right]_{z'=0}\\ &= \frac{I}{2\pi}\left\{\mathrm{i}k\coth\left(\frac{\mathrm{i}kc}{2}\right)\ln\rho - \frac{4}{c}\sum_{\nu=1}^{\infty}\frac{(2\pi\nu)^2}{(2\pi\nu)^2-(kc)^2}\right.\\ &\qquad\left.\times K_0\left[(\rho/c)\sqrt{(2\pi\nu)^2-(kc)^2}\right]\cos(2\pi\nu z/c)\right\}.\end{aligned} \tag{3.39}$$

At the plate surface $z=0$, the cosine term in the summation becomes unity and the potential drop can be written as in equation (3.36) where now

$$f_p(\rho) = -\mathrm{i}k\coth\left(\frac{\mathrm{i}kc}{2}\right)\ln\rho + \frac{4}{c}\sum_{\nu=1}^{\infty}\frac{(2\pi\nu)^2}{(2\pi\nu)^2-(kc)^2}K_0\left[(\rho/c)\sqrt{(2\pi\nu)^2-(kc)^2}\right]. \tag{3.40}$$

(*g*) *Thin-plate approximation*

It is possible to show that only the first term on the right-hand side of equation (3.40) is significant when the plate thickness $c/2$ is somewhat smaller than the separation between the probe points, $\sim\rho_{ij}$. Two dimensionless length parameters are present in the expression: kc and ρ/c. When $\rho/c \gg 1$, the summation term is smaller than that containing the factor of $\ln\rho$ for all values of k. This can be seen by considering the asymptotic behaviour of K_0. For large argument $|z|$, the following asymptotic expansion for $K_0(z)$ holds:

$$K_\zeta(z) = \sqrt{\frac{\pi}{2z}}e^{-z}\left(1+\frac{\mu-1}{8z}+\dots\right), \quad |\arg z| < 3\pi/2, \tag{3.41}$$

in which ζ is fixed, $|z|$ is large and $\mu = 4\zeta^2$ (eqn (9.7.2) in the work of Abramowitz & Stegun (1970)). Hence, taking the first term in the above series,

$$K_0(z) \approx \sqrt{\frac{\pi}{2z}} e^{-z}, \quad |z| \gg 1. \tag{3.42}$$

For $k=0$ and $k \to 0$, the terms of the summation on the right-hand side of equation (3.40) contain the factors $\exp(-2\pi\nu\rho/c)$ and $\exp(-ik\rho)$, respectively. These exponential factors are sufficient to render the summation significantly smaller than the first term on the right-hand side of equation (3.40) and

$$f_{\mathrm{tp}}(\rho) \approx -ik \coth\left(\frac{ikc}{2}\right) \ln \rho, \quad c/\rho \ll 1. \tag{3.43}$$

In the work of Bowler & Huang (2005*a*), the electrical conductivity, effective magnetic permeability and the thickness of brass, aluminium, stainless steel, spring steel and carbon steel plates have been determined by inverting measurement data using formula (3.43). In the work of Bowler (2006*b*), the accuracy of this formula is investigated as a function of plate thickness and probe point separations, in the limit of zero frequency (direct current). Theoretically speaking, equation (3.43) becomes more accurate as the pickup points are moved further away from the current input points, although practically this reduces the strength of the measured voltage, which may adversely affect the overall accuracy of the measurement.

4. Summary of theoretical results

For ease of reference, the theoretical results developed in the previous sections are collected and summarized here. In general, the ACPD measured between the two pickup points of a four-point probe in contact with a conductive surface can be written as

$$V = \frac{I}{2\pi\sigma}[F_k(\rho_{22}) - F_k(\rho_{21}) - F_k(\rho_{12}) + F_k(\rho_{11})], \tag{4.1}$$

where $F_{\mathrm{k}}(\rho)$ can take several forms. In the case of a half-space conductor, F_{hs} is obtained by summing f_ε, (equation (2.9)) and f_{hs} (equation (3.28)) to give

$$F_{\mathrm{hs}}(\rho) = \frac{e^{ik\rho}}{\rho} + ik\left[E_1(-ik\rho) + \left(1 - \frac{ikh}{\mu_{\mathrm{r}}}\right)\ln \rho\right]. \tag{4.2}$$

This result agrees with eqn (31) in the work of Bowler (2006*a*). In the case of a plate, F_{p} is obtained by summing f_ε (equation (2.9)) and either representation for f_{p} (equation (3.37) or (3.40)) to give

$$F_{\mathrm{p}}(\rho) = -ik\left[\coth\left(\frac{ikc}{2}\right) + \frac{ikh}{\mu_{\mathrm{r}}}\right]\ln \rho + \sum_n \left(\frac{\exp\left[ik\sqrt{\rho^2 + (nc)^2}\right]}{\sqrt{\rho^2 + (nc)^2}} + ike^{iknc} E_1\left\{-ik\left[\sqrt{\rho^2 + (nc)^2} - nc\right]\right\}\right), \tag{4.3}$$

or

$$F_{\mathrm{p}}(\rho) = -\mathrm{i}k\left[\coth\left(\frac{\mathrm{i}kc}{2}\right) + \frac{\mathrm{i}kh}{\mu_{\mathrm{r}}}\right]\ln\rho + \frac{4}{c}\sum_{\nu=1}^{\infty}\frac{(2\pi\nu)^2}{(2\pi\nu)^2-(kc)^2}K_0\left[(\rho/c)\sqrt{(2\pi\nu)^2-(kc)^2}\right]. \tag{4.4}$$

The first of these summations, equation (4.3), converges more rapidly for thick plates, whereas the second, equation (4.4), converges more rapidly for thin plates. Finally, an approximation for plates somewhat thinner than the probe point separations, F_{tp}, can be written as a sum of f_ε (equation (2.9)) and f_{tp} (equation (3.43)) to give

$$F_{\mathrm{tp}}(\rho) \approx -\mathrm{i}k\left[\coth\left(\frac{\mathrm{i}kc}{2}\right) + \frac{\mathrm{i}kh}{\mu_{\mathrm{r}}}\right]\ln\rho, \quad c/\rho \ll 1, \tag{4.5}$$

in agreement with eqn (9) in the work of Bowler & Huang (2005*a*).

5. Example calculations

While the theory developed above is applicable for arbitrary relative placement of the four probe points on the plate surface, in this section a collinear arrangement of the probe points is considered, with equal separation between the points. The length of the probe is $2s$ and the plate thickness is here denoted T (figure 4). For a discussion of the effects of changing the spacing between the probe points, for collinear and rectangular point arrangements in the limit of direct current, see the work of Bowler (2006*b*).

(*a*) *Accuracy of the thin-plate approximation*

Figure 5 compares the dimensionless pickup voltage $\pi\sigma vs/I$, plotted as a function of dimensionless frequency $\omega\mu\sigma s^2$, calculated using the AC plate solution given by equations (4.1) and (4.3) together and with the thin-plate approximation of equation (4.5). The contribution to the voltage due to induction in the pickup circuit (f_ε) is excluded from this comparison by putting $h=0$. Also shown is the DC plate solution presented in the work of Bowler (2006*b*), which may be obtained by taking the limit $k\to 0$ either in equation (4.3) or in equation (4.4),

$$\lim_{k\to 0} F_{\mathrm{p}}(\rho) = \sum_n \frac{1}{\sqrt{\rho^2 + (2nT)^2}}. \tag{5.1}$$

Comparisons are shown for a plate with the same thickness as the probe length, $T=2s$, and for a plate with thickness one-quarter of the probe length, $T=s/2$. For the thicker plate, only one term in the series in equation (4.3) was required for convergence, i.e. $N=0$ and the system behaves as a half space. For the thinner plate, $N=25$ for 2% accuracy in the calculation. From the figure, it can be seen that there is a quasi-static regime in which the AC voltage agrees with that of the DC limit. The upper bound of this regime depends on the plate thickness. The thin-plate approximation matches the voltage calculated using the full plate solution quite well (to within 2.5%) for $T=s/2$, whereas for $T=2s$ the thin-plate approximation underestimates the voltage by around 50%.

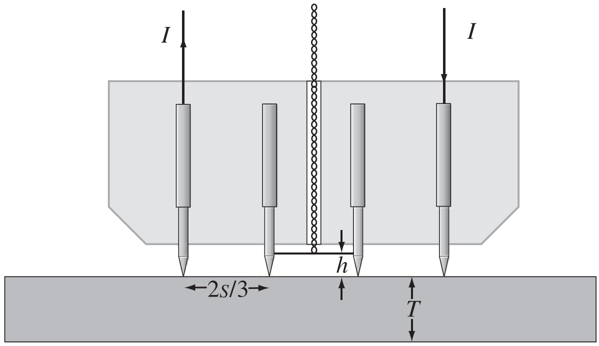

Figure 4. Collinear probe with length $2s$ and equally spaced probe points.

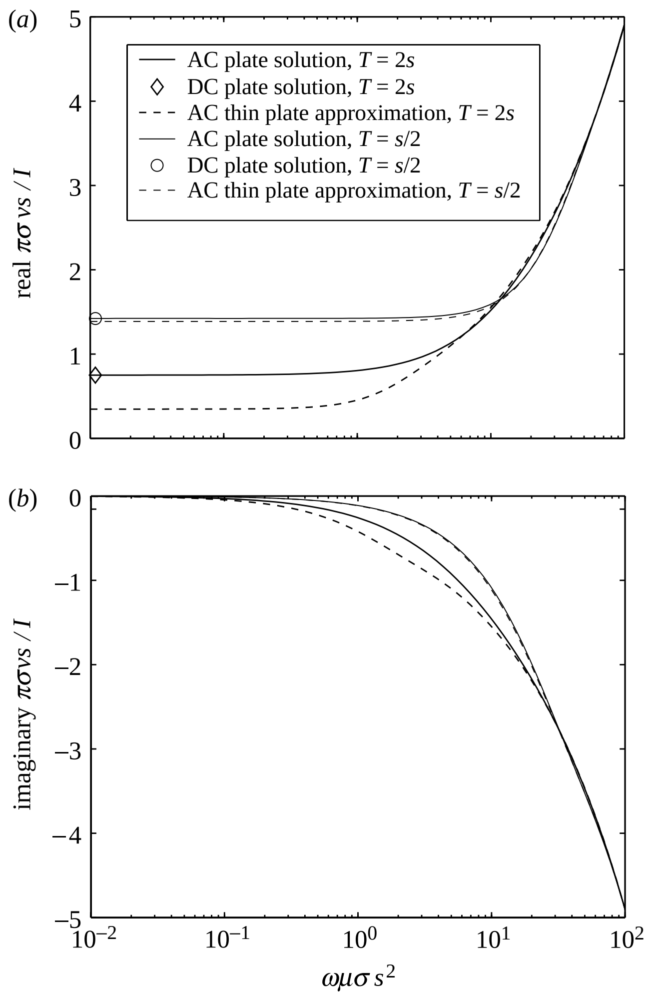

Figure 5. Dimensionless pickup voltage, $\pi\sigma vs/I$, as a function of dimensionless frequency, $\omega\mu\sigma s^2$, in the case of a collinear probe with equal point spacing, for $T{=}2s$ and $T{=}2/s$.

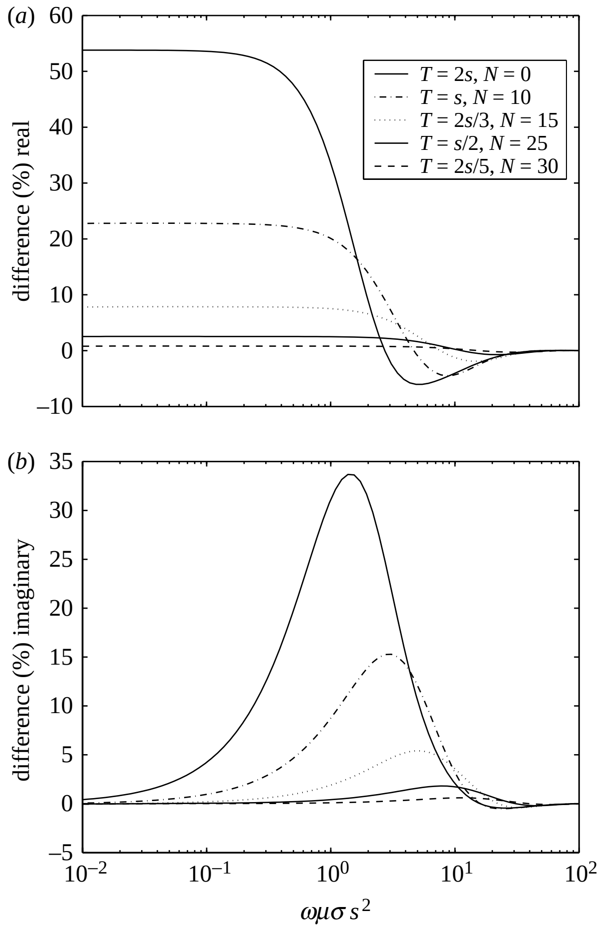

Figure 6. Percentage difference between pickup voltages calculated using the full plate solution given in equation (4.3) and thin-plate approximation (4.5), for various ratios of the probe length $2s$ to the plate thickness T. N is the number of terms required in the series of equation (4.3) to give accuracy ± 0.03 in the plotted percentage $h=0$.

The agreement between the thin-plate approximation and the full plate solution is investigated further in figure 6, where the percentage difference defined,

$$\frac{F_{\rm p}-F_{\rm tp}}{F_{\rm p}}\times 100, \tag{5.2}$$

is plotted as a function of frequency for various plate thicknesses. The largest difference between the theoretical values occurs in the real part of the voltage in the quasi-static regime (the low-frequency asymptote). The percentage difference for each plate thickness considered is listed in table 1. It is clear that the thin-plate approximation can be used to better than 1% accuracy for plates whose thickness is one-fifth or less of the probe length, for this case of equal electrode spacing in a collinear probe.

Table 1. Difference between the full plate solution and the thin-plate approximation. Quasi-static voltage values are compared. $T/(2s)$ is the ratio of the plate thickness to the probe length. The probe is a collinear probe with equal electrode spacing. N is the number of terms required in the series of equation (4.3) to give accuracy ± 0.03 in the percentage difference.

$T/(2s)$	N	difference (%)
1	0	54
1/2 (0.5)	10	23
1/3 (0.333)	15	7.8
1/4 (0.25)	25	2.5
1/5 (0.2)	30	0.80

Table 2. Number of terms required for convergence of series solutions. Number of terms, N, needed in each of the series in equations (4.3) and (4.4) to give agreement within 0.1% in the calculated potential drop for a probe with equally spaced points in contact with a conductive plate with thickness T.

$T/(2s)$	N, series (4.3)	N, series (4.4)
1	3	7
3/4 (0.75)	4	4
1/2 (0.5)	6	3
1/3 (0.333)	8	2
1/4 (0.25)	10	1
1/5 (0.2)	12	1

(*b*) *Convergence of Fourier series expansion*

In table 2, the number of terms required to give 0.1% agreement between potential drops calculated using the alternative series expansions (4.3) and (4.4) are given for a variety of plate thicknesses. Again, the probe points are collinear and equally spaced. It is clear from the table that a similar number of terms are needed in each series for a plate with thickness approximately three-quarters the probe length. Either side of this thickness, the number of terms needed for convergence of each of these series differs significantly. For larger T, computation of the series in equation (4.3) is more efficient. For smaller T, equation (4.4) should be used.

6. Experimental validation of the theory

Experimental validations have already been performed in the thin-plate regime (Bowler & Huang 2005*a*) and for a conductive half space (Bowler 2006*a*). In figure 7, the experimental data are compared with the theory for a titanium plate whose thickness is similar to the length of a collinear probe, $T/(2s) \approx 2/3$. The probe and the plate parameters are given in tables 3 and 4, respectively. The lateral dimensions of the plate are large, to avoid the influence of the plate edges on the measurements. Details of the experimental procedure for the ACPD

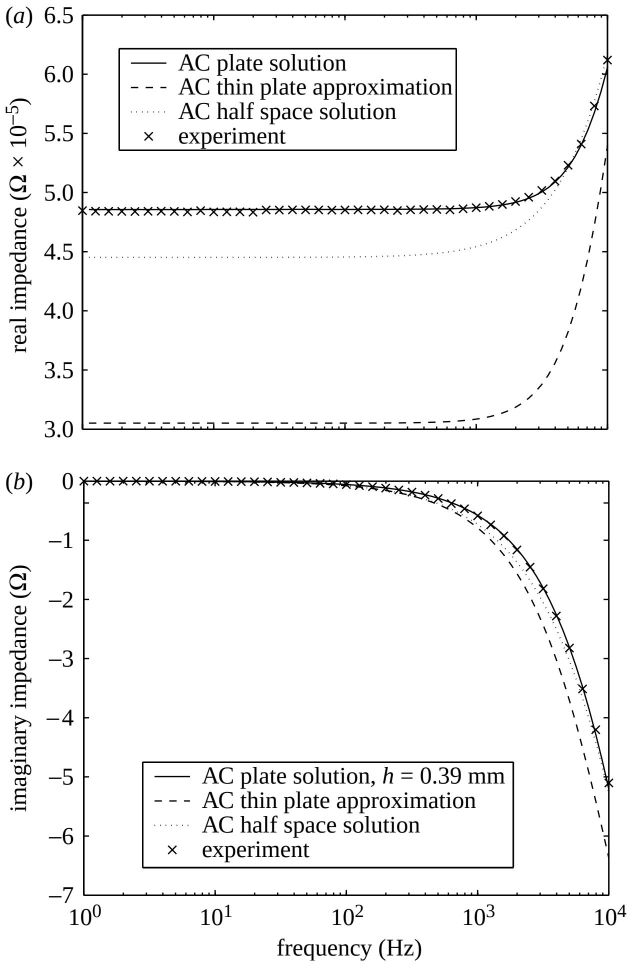

Figure 7. Impedance (V/I) measured by a collinear four-point probe (table 3) in contact with a titanium plate (table 4), compared with the theory expressed in equation (4.3) (with N=12) and the thin-plate approximation of equation (4.5), as a function of frequency. The solution for a half-space conductor is also shown (equation (4.2)).

measurements are available in the works of Bowler & Huang (2005*a*,*b*). There is very good agreement between the AC plate theory expressed in equations (4.1) and (4.3), N=12, and the experimental data. The value of h, the vertical dimension of the pickup loop from the surface of the test piece, has been adjusted in the theory to give the best fit to the imaginary part of the experimental data. The value obtained, h=0.39 mm, is similar to that measured physically. There are no adjustable parameters in the calculation of the real part of the impedance. Also shown in figure 7 are the theoretical curves calculated for a conductive half space (equation (4.2)) and using the thin-plate approximation (4.5). It is clear that this experiment occupies a regime in which neither of those solutions agrees well with the experimental data. Rather, the solution for arbitrary plate thickness is validated successfully.

Table 3. Probe parameters (for a collinear probe with length $2s$.)

$2s$ (mm)	voltage electrode separation (mm)	h (mm) (fitted value)
18.49 ± 0.005	6.16 ± 0.005	0.39 ± 0.01

Table 4. Plate parameters. Conductivity, σ; thickness, T and lateral dimensions $w \times d$. σ was measured in the work of Bowler (2006*b*) via the four-point probe method described in the work of Bowler & Huang (2005*b*). The plate thickness was determined from the average of several measurements using digital callipers.

metal	alloy	σ (MSm^{-1})	T (mm)	$w \times d$ (mm)
titanium	Ti-6Al-4V	0.58 ± 0.01	12.47 ± 0.01	318×331

7. Conclusion

Analytic solutions are derived for the complex potential drop measured between the two points of a four-point probe placed on the surface of a homogeneous metal plate. Alternating current is injected into the plate via the other two probe points. The relative arrangement of the four probe points is not restricted in the theoretical development. Two series solutions are derived. The first converges rapidly for plates that are somewhat thicker than the separation of the probe points and reduces to the solution for a half-space conductor. The second converges rapidly for plates somewhat thinner than the separation of the probe points.

The existence of these analytic solutions permits non-destructive determination of the plate thickness, electrical conductivity and linear effective magnetic permeability by inversion of measured data. Briefly, from a single spectrum of measured ACPD data, either the plate thickness or its conductivity can be inferred from the low-frequency (quasi-static) portion of the spectrum, in which the measured voltage is real, constant and independent of magnetic permeability (Bowler & Huang 2005*b*). Then, higher-frequency data can be inverted to obtain a value for the linear effective magnetic permeability (Bowler & Huang 2005*b*).

The authors acknowledge the assistance of J. T. Brown in obtaining the experimental data shown in figure 7. This work was supported by the NSF Industry/University Cooperative Research Program.

References

Abramowitz, M. & Stegun, I. A. (eds) 1970 *Handbook of mathematical functions with formulas, graphs and mathematical tables*. New York, NY: Dover Publications, Inc. 9th printing.

Bowler, N. 2004*a* Analytical solution for the electric field in a half-space conductor due to alternating current injected at the surface. *J. Appl. Phys.* **95**, 344–348. (doi:10.1063/1.1630700)

Bowler, N. 2004*b* Electric field due to alternating current injected at the surface of a metal plate. *J. Appl. Phys.* **96**, 4607–4613. (doi:10.1063/1.1793332)

Bowler, N. 2006*a* Theory of four-point alternating current potential drop measurements on a metal half-space. *J. Phys. D: Appl. Phys.* **39**, 584–589. (doi:10.1088/0022-3727/39/3/024)

Bowler, N. 2006*b* Theory of four-point direct-current potential drop measurements on a metal plate. *Res. Nondestr. Eval.* **17**, 29–48. (doi:10.1080/09349840600582092)

Bowler, N. & Huang, Y. 2005*a* Model-based characterization of homogeneous metal plates using four-point alternating current potential drop measurements. *IEEE Trans. Magn.* **41**, 2102–2110. (doi:10.1109/TMAG.2005.847625)

Bowler, N. & Huang, Y. 2005*b* Electrical conductivity measurement of metal plates using broadband eddy-current and four-point methods. *Meas. Sci. Technol.* **16**, 2193–2200. (doi:10.1088/0957-0233/16/11/009)

Dover, W. D., Charlesworth, F. D. W., Taylor, K. A., Collins, R. & Michael, D. H. 1981 The use of A-C field measurements to determine the shape and size of a crack in a metal. In *Eddy-current characterization of materials and structures, ASTM STP 722* (eds G. Birnbaum & G. Free), pp. 401–427. Philadelphia, PA: American Society for Testing and Materials.

Gradshteyn, I. S. & Ryzhik, I. M. 2000 *Table of integrals, series and products*, 6th edn. San Diego, CA: Academic Press.

Hwang, I. S. & Ballinger, R. G. 1992 A multi-frequency AC potential drop technique for the detection of small cracks. *Meas. Sci. Technol.* **3**, 62–74. (doi:10.1088/0957-0233/3/1/009)

Michael, D. H., Waechter, R. T. & Collins, R. 1982 The measurement of surface cracks in metals by using AC electric fields. *Proc. R. Soc. A* **381**, 139–157.

Sperb, R. 1996 An alternative to Ewald sums—part I: identities for sums. Report no. 96-18, Seminar für Angewandte Mathematik, Eidgenössische Technische Hochschule, Zürich, Switzerland.